A supercritical density of fast Na^+ channels ensures rapid propagation of action potentials in GABAergic interneuron axons

Hua Hu & Peter Jonas

IST Austria (Institute of Science and Technology Austria), Am Campus 1, A-3400 Klosterneuburg, Austria

Corresponding authors:
Dr. Peter Jonas
Dr. Hua Hu
IST Austria
Am Campus 1
A-3400 Klosterneuburg
Austria
Phone: ++43-2243-9000-3701
Fax: ++43-2243-9000-2007
E-mail: peter.jonas@ist.ac.at, hua.hu@ist.ac.at

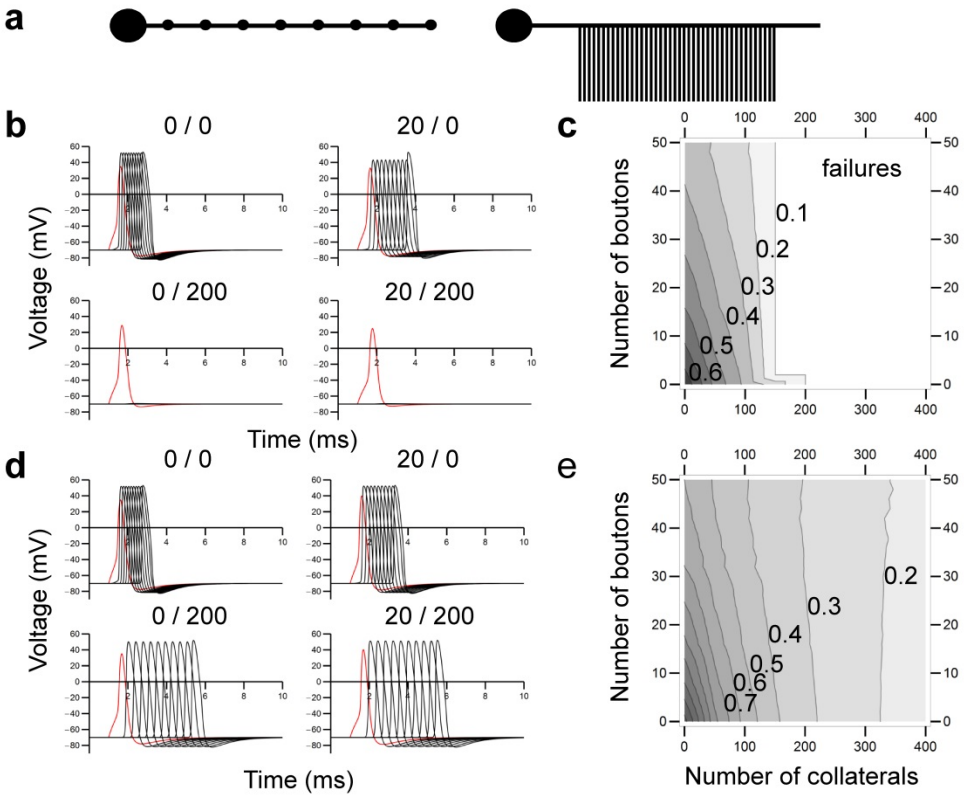

Supplementary Figure 1 High density of boutons and axon collaterals generates failures and slowing of propagation of APs in schematic models.

(**a**) Structure of the schematic model. Large sphere on the left represents soma (20 µm diameter), horizontal cylinder on the right is axon (1 mm length; 0.5 µm diameter), small spheres represent boutons (5 µm diameter), and vertical cylinders indicate axon collaterals (100 µm length; 0.3 µm diameter). Throughout the simulations, $\overline{g_{Na}}$ in the soma was 200 pS µm^{-2}, and $\overline{g_{Na}}$ in the axon was 1200 pS µm^{-2}. Boutons and collaterals were introduced with equidistant spacing. Axon diameters were approximately consistent with previous electron microscopy data[14].

(**b**) APs evoked by a short current pulse at the soma (1 nA, 1 ms). Red trace, somatic AP, black traces, APs in the axon at different sites with 100 µm distance. Numbers on top indicate the number of boutons / number of collaterals.

(**c**) Contour plot of AP propagation velocity against number of boutons and number of axon collaterals. Note failure of AP propagation in a large part of the parameter space. In both **b** and **c**, passive properties of boutons and collaterals were assumed ($\overline{g_{Na}}$ = 0).

(**d, e**) AP traces (**d**) and contour plot of AP propagation velocity (**e**) in the case of active boutons and collaterals ($\overline{g_{Na}}$ = 1200 pS µm^{-2}).

Numbers right-adjacent to contour lines in **c** and **e** indicate AP propagation velocity (in m s^{-1}).

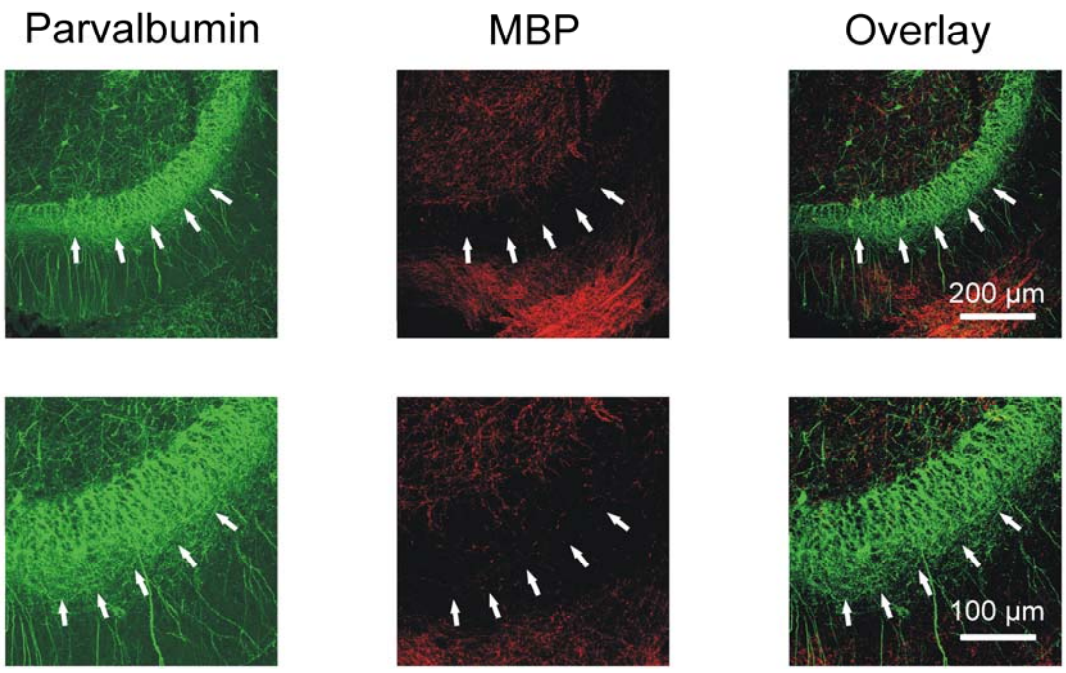

Supplementary Figure 2 Minimal myelination of BC axons in dentate gyrus of 6-weeks-old rats. Double immunolabeling for parvalbumin and myelin basic protein (MBP) in a 6-week-old rat. Left, parvalbumin; center, MBP; right, overlay. Note the absence of colocalization between the two markers in the granule cell layer, suggesting that BC axons are largely unmyelinated. Experiments were repeated on 5 animals, giving consistent results. White arrows indicate the outer border of the granule cell layer. Lower micrographs are expanded versions of upper images.

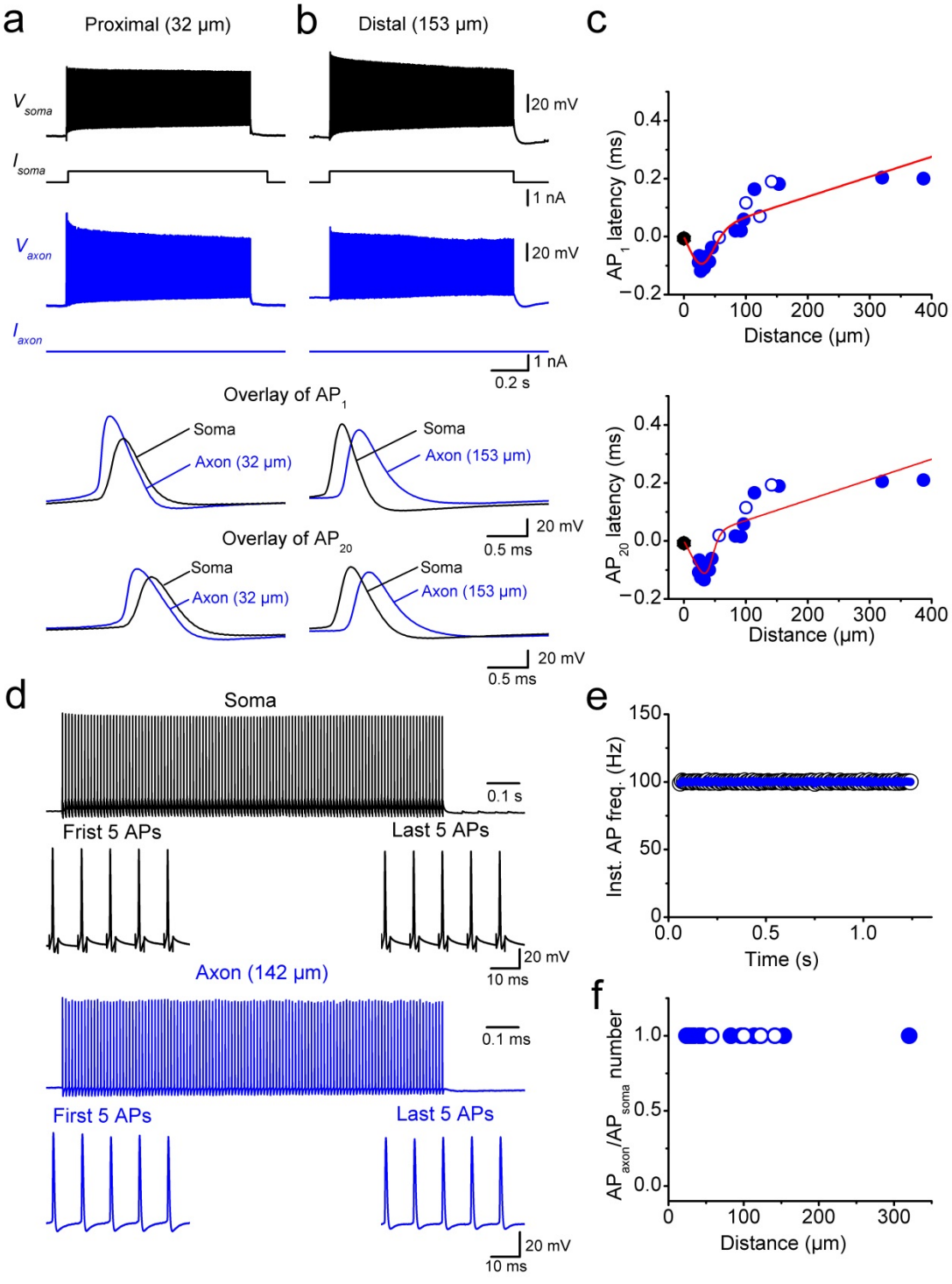
a
Proximal (32 μm)
b
Distal (153 μm)
c
V_{soma}
I_{soma}
V_{axon}
I_{axon}
20 mV
1 nA
20 mV
1 nA
0.2 s
Overlay of AP_1
Soma
Axon (32 μm)
Soma
Axon (153 μm)
20 mV
0.5 ms
Overlay of AP_{20}
Soma
Axon (32 μm)
Soma
Axon (153 μm)
20 mV
0.5 ms
AP_1 latency (ms)
Distance (μm)
AP_{20} latency (ms)
Distance (μm)
d
Soma
0.1 s
Frist 5 APs
Last 5 APs
20 mV
10 ms
Axon (142 μm)
0.1 ms
First 5 APs
Last 5 APs
20 mV
10 ms
e
Inst. AP freq. (Hz)
Time (s)
f
AP_{axon}/AP_{soma} number
Distance (μm)

Supplementary Figure 3 Proximal initiation and fast, reliable propagation of APs in interneuron axons at near-physiological temperature.
(**a, b**) Simultaneous recording from the soma and the axon of a fast-spiking, parvalbumin-expressing BC during a long somatic current pulse. Black, somatic voltage; blue, axonal voltage. The axonal recording site was located 32 µm (**a**) or 153 µm (**b**) from the soma. Bottom traces show expanded views of the first and the 20th AP in the high-frequency train. Black traces, somatic voltage and corresponding current; blue traces, axonal voltage and corresponding current.
(**c**) Plot of latency between somatic and axonal AP against distance of the axonal recording site from the soma for the first AP (upper graph) and the 20th AP (lower graph). Data from 19 simultaneous axon–soma recordings. Filled circles, recordings from axon varicosities; open circles, recordings from axon shafts; red line, bilinear function fit to the data points.
(**d**) Simultaneous recording from the soma and the axon of a BC during a high-frequency train of short somatic current pulses (100 Hz, 120 stimuli; 3 ms, 1 nA). Black, somatic voltage; blue, axonal voltage. The axonal recording site was located 142 µm from the soma.
(**e**) Plot of instantaneous somatic and axonal AP frequency during the stimulation train. The axonal AP frequency was 100 Hz, identical to the stimulation frequency.
(**f**) Plot of ratio of number of APs in the axon over number of APs in the soma, plotted against distance of the axonal recording site. Data from 18 simultaneous axon–soma recordings. Note that the ratio was 1 in all cases, indicating high reliability of propagation.

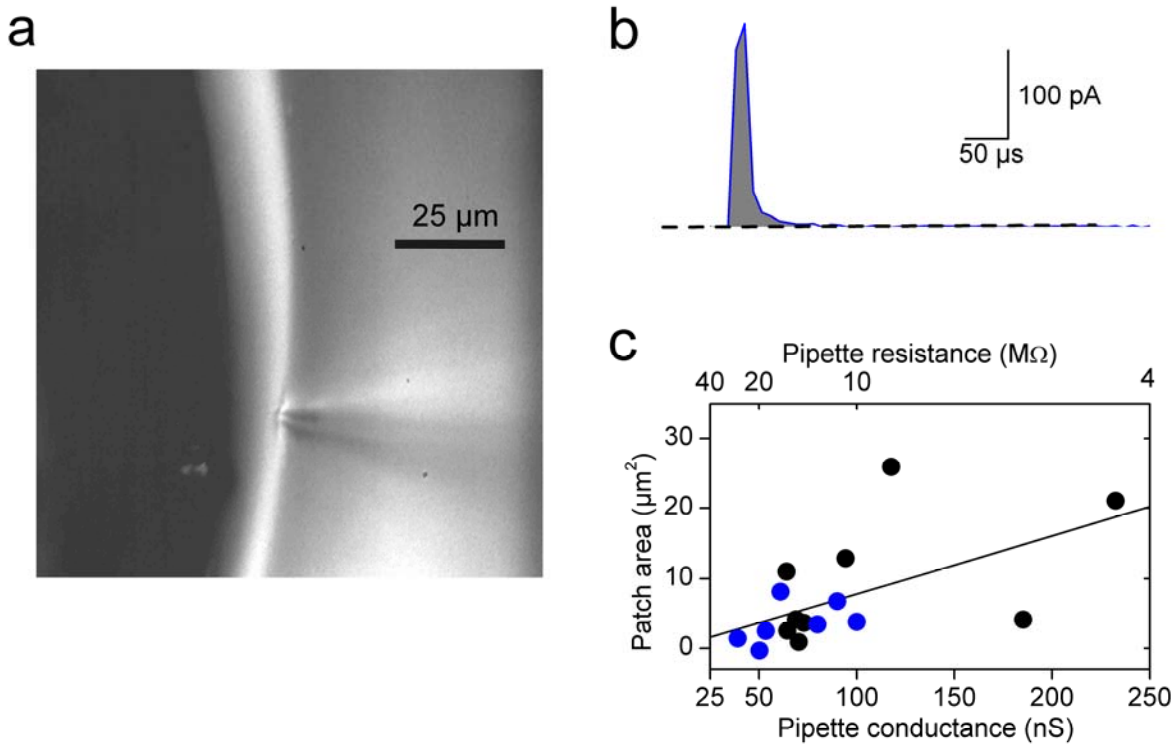

Supplementary Figure 4 Patch area determined by capacitance measurements.
(**a**) Experimental configuration. The silicone elastomer ball is visible on the left, the patch pipette is located on the right. The pipette tip was gently pushed into the insulating ball, with an insertion depth of ~10 µm.
(**b**) Difference current before and after pressing the pipette tip with the outside-out patch into the Sylgard ball. Shaded area indicates integral under the current trace. Currents were evoked by a test pulse to –100 mV from a holding potential of –50 mV.
(**c**) Plot of patch area against pipette conductance. Data were fit by linear regression, with the parameters $A(g_P) = 0.08271 \times g_P - 0.47526$, where A is patch area (μm^2) and g_P is pipette conductance (nS). Patch area was calculated from capacitance, assuming a specific membrane capacitance of 1 µF cm^{-2}. The upper horizontal axis shows pipette resistance (which is the inverse of pipette conductance). Results were obtained from 7 axonal and 9 somatic outside-out patches. Somatic data are shown in black, axonal data are depicted in blue.

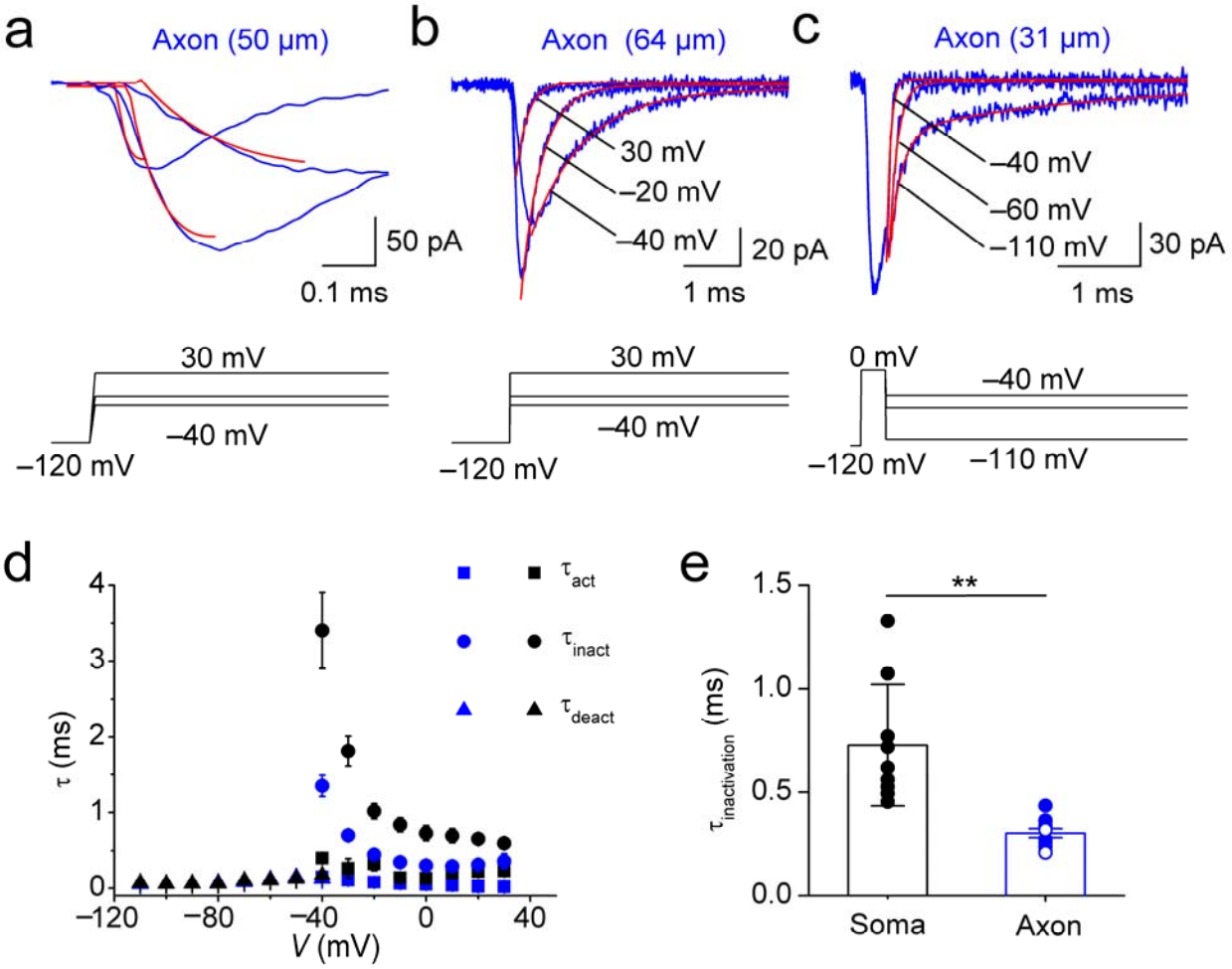

Supplementary Figure 5 Fast gating of Na^+ channels in BC axons.
(**a**–**c**) Activation (**a**), inactivation (**b**), and deactivation time course of axonal Na^+ channels (**c**). Outside-out patches isolated from the axon 50, 64, and 31 µm from the soma. Red curves indicate exponential functions fit to the recorded traces. The corresponding pulse protocol is shown at the bottom.
(**d**) Plot of activation (squares), inactivation (circles), and deactivation time constants (triangles) against test pulse potential.
(**e**) Summary bar graph of inactivation time constant at 0 mV. Bars indicate mean ± SEM, circles represent data from individual experiments (9 somatic and 11 axonal patches). Note the marked difference in the inactivation time constants between somatic and axonal Na^+ channels. ** indicates $P < 0.01$. Somatic data are shown in black, axonal data are depicted in blue.

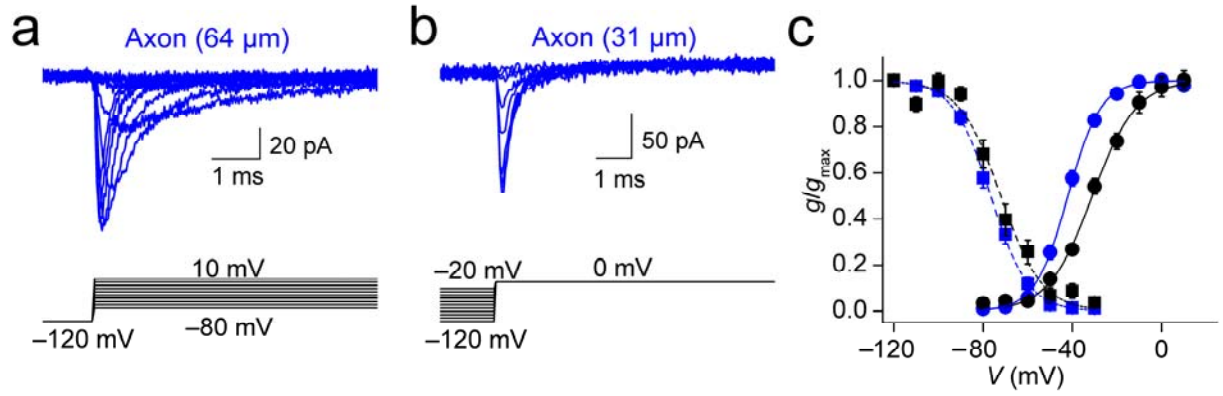

Supplementary Figure 6 Negative shift of voltage-dependence of Na^+ channel activation and inactivation in BC axons.
(**a**) Na^+ currents in an outside-out patch isolated from the axon 64 µm from the soma. The corresponding activation pulse protocol with increasing test pulse amplitude is shown at the bottom.
(**b**) Na^+ currents in an outside-out patch isolated from the axon 31 µm from the soma. The corresponding inactivation pulse protocol with increasing prepulse amplitude is shown at the bottom.
(**c**) Na^+ channel activation and inactivation curves. Data points indicate mean ± SEM from 6–14 patches. Data points were fit with Boltzmann functions. Note that the activation curve of axonal Na^+ channels is shifted to the left in comparison to that of somatic Na^+ channels. Somatic data are shown in black, axonal data are depicted in blue. Continuous and dashed lines represent Boltzmann functions fit to activation and inactivation data points, respectively.

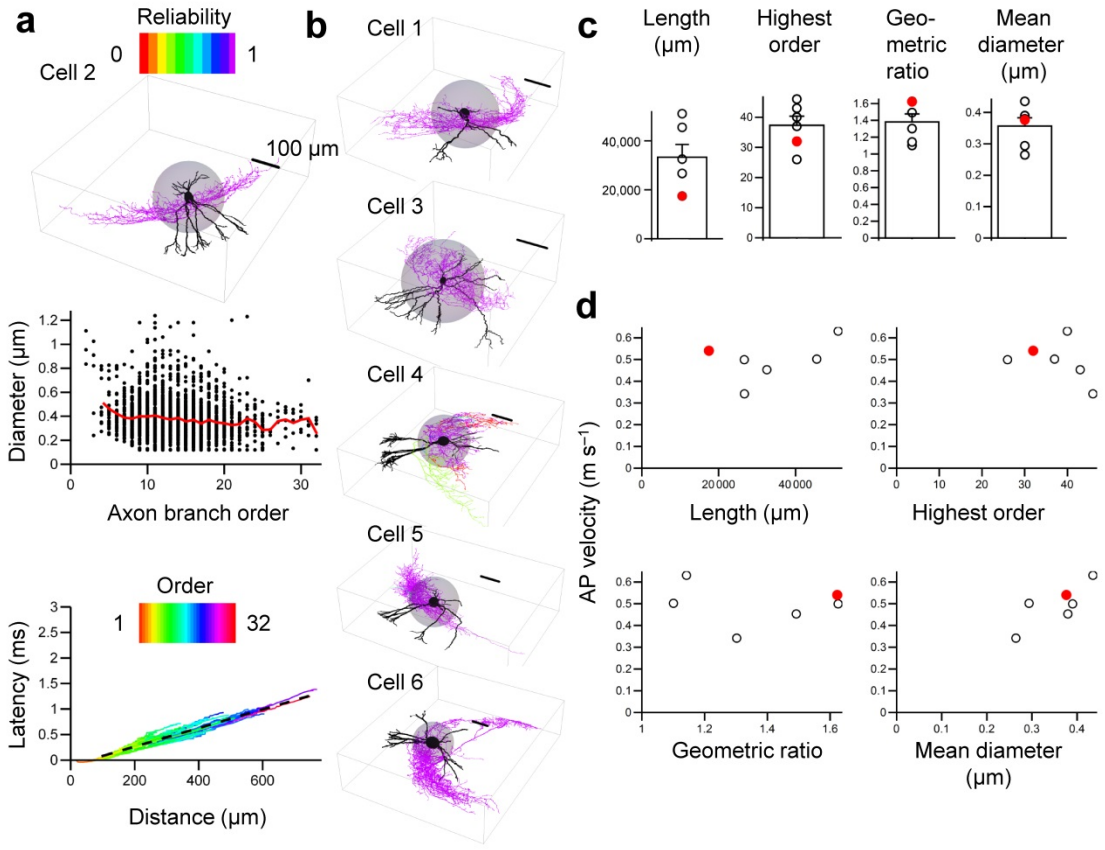

Supplementary Figure 7 Dependence of reliability and velocity of AP propagation on axonal Na^+ conductance density is independent of details of morphological properties.
(**a**) AP propagation in cell 2, used for the computational analysis in Fig. 4. Top, plot of reliability of AP propagation, shown as color coding of the surface of the reconstructed neuron for proximal $\overline{g_{Na}}$ = distal $\overline{g_{Na}}$ = 500 pS µm^{-2}. Color scale bar indicates the reliability of propagation in the axon (inset, top).
Center, plot of axon diameter against axon branch order. Black points indicate diameters of individual sections, red line represents mean.
Bottom, plot of latency against distance. Note that the slope of the latency–distance relation is constant over a wide range of distances and branch orders, indicating constant AP propagation velocity. Proximal $\overline{g_{Na}}$ = distal $\overline{g_{Na}}$ = 1000 pS µm^{-2}. Dashed line indicates the results of linear regression for distances > 100 µm. Color scale bar indicates axon branch order (inset, top).
(**b**) AP propagation in 5 other fully reconstructed BCs. Note that all cells except one (cell 4, center) showed absolute reliability of propagation; proximal $\overline{g_{Na}}$ = distal $\overline{g_{Na}}$ = 500 pS µm^{-2}.
(**c**) Structural properties of BC axons in the fully reconstructed cells. Bars indicate mean ± SEM, circles represent data from individual experiments.
(**d**) Plot of AP propagation velocity against structural parameters of BC axons. Red points in **c** and **d** indicate cell 2 used for the simulations in Fig. 4. This cell was chosen because its axon diameter was most representative.

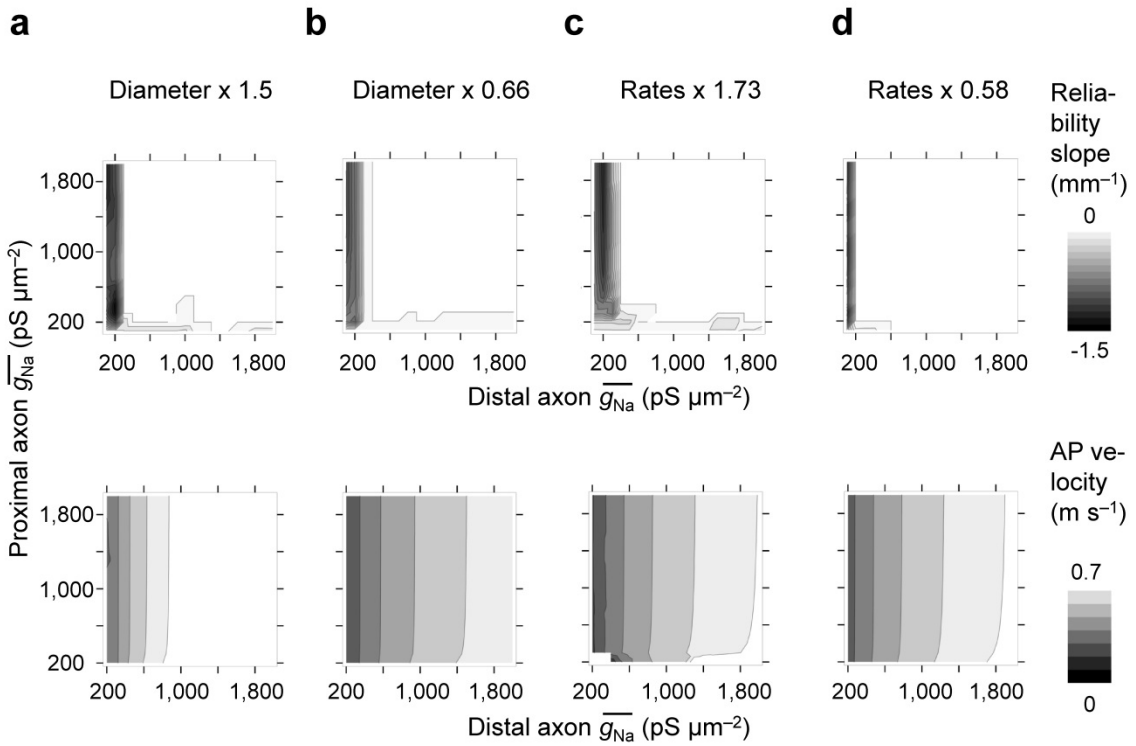

Supplementary Figure 8 Dependence of reliability and velocity of AP propagation on axon diameter and channel gating kinetics.
(**a**) Effects of increase in axon diameter (multiplying all diameters by a factor of 1.5).
(**b**) Effects of decrease in axon diameter (multiplying all diameters by a factor of 0.66).
(**c**) Effects of accelerating Na^+ channel inactivation rates and K^+ channel activation rates (multiplying corresponding rates by a factor of 1.73, corresponding to a 5°C temperature increase for a Q_{10} of 3).
(**d**) Effects of slowing Na^+ channel inactivation rates and K^+ channel activation rates (multiplying corresponding rates by a factor of 0.58, corresponding to a 5°C temperature decrease for a Q_{10} of 3).
Upper graphs, contour plots of the average slope of the reliability–distance relation as a function of proximal and distal $\overline{g_{Na}}$.
Lower graphs, contour plots of AP propagation velocity as a function of proximal and distal $\overline{g_{Na}}$.
Gray scale bar indicates the value of the indicated parameter (right). All simulations were performed on cell 2. Parameters of the simulations were identical to those in Fig. 4, unless specified differently.

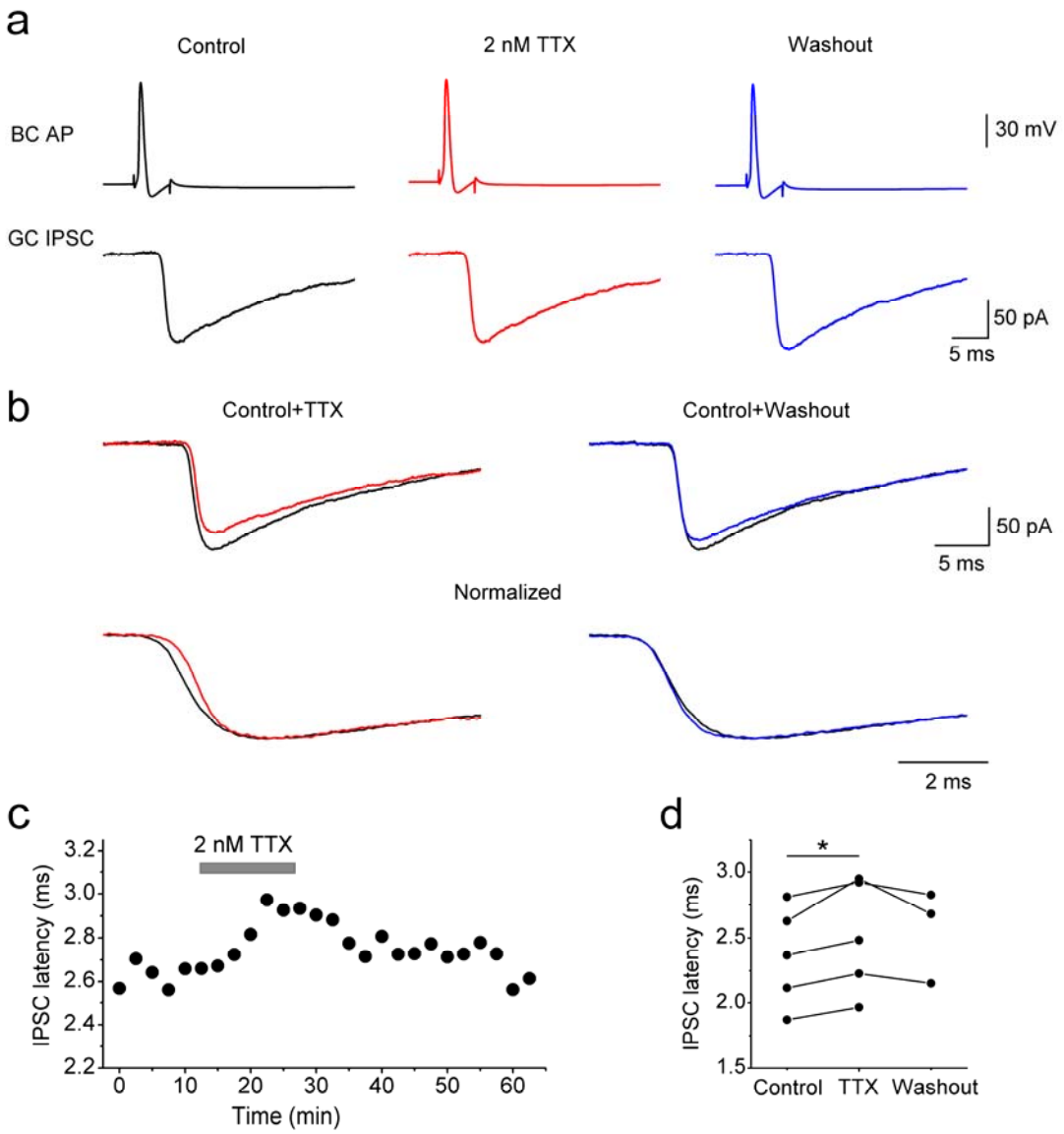

Supplementary Figure 9 Partial block of Na^+ channels increases latency of evoked IPSCs at BC–GC synapses.

(**a**) Unitary IPSCs at BC–GC synapses under control conditions (left), in the presence of 2 nM TTX in the bath (center), and after washout (right). Upper traces, APs in BCs evoked by brief current pulses; bottom traces, average IPSCs.

(**b**) Overlay of traces in control and 2 nM TTX (left) and control and washout (right) at different time scales. Note that 2 nM TTX reversibly increased the latency of evoked IPSCs. Upper traces are displayed at absolute current scale, lower traces are shown normalized to the same peak amplitude to facilitate comparison of synaptic latency.

(**c**) Plot of IPSC latency against experimental time during application of 2 nM TTX (horizontal bar) from the same experiment as shown in (**a, b**). Each data point represents the mean of 25 consecutive IPSC latency values.

(**d**) Summary graph of the effects of 2 nM TTX on IPSC latency. Data from 5 BC–GC pairs. Data from the same experiment were connected by lines. * indicates $P < 0.05$. Slight differences in the 20–80% rise time (**b**) were not significant ($P > 0.1$).

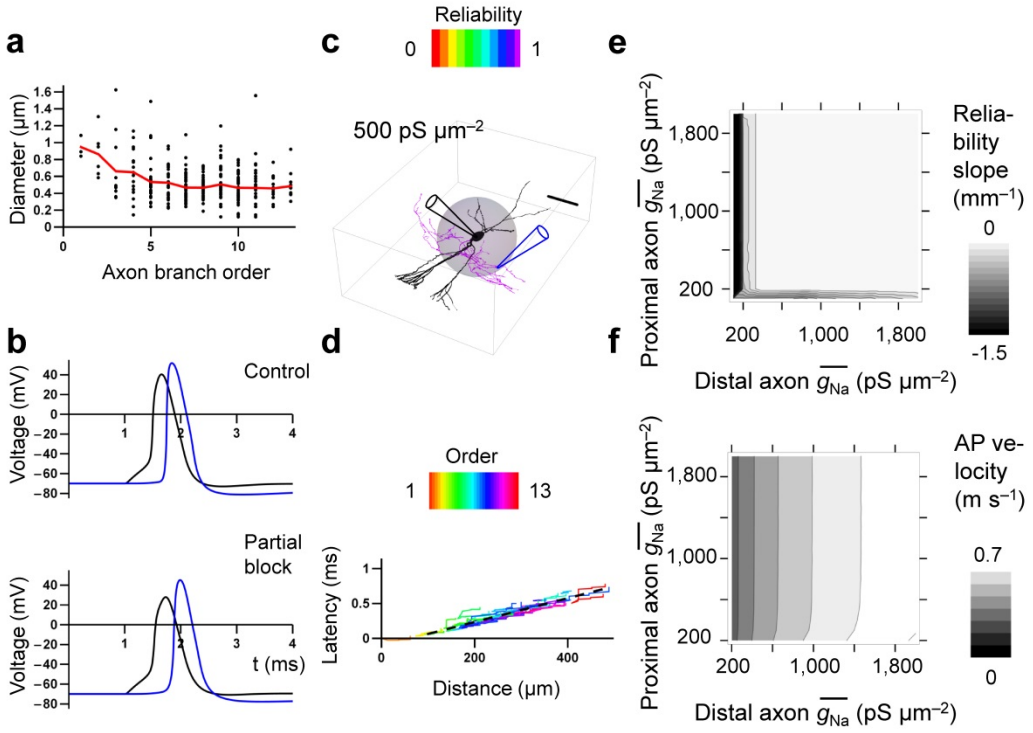

Supplementary Figure 10 A supercritical Na^+ channel density in the axon ensures fast AP propagation in an experimentally recorded cell.
(**a**) Plot of axon diameter against axon branch order in the experimentally recorded cell. Same cell as shown in **Fig. 5d**, open circles. Black points indicate diameter of individual sections, red line represents mean. Note that the axon could be only partially reconstructed.
(**b**) Simulated APs at the soma (black) and the axonal recording site (blue) under control conditions (top) and after simulated block of 43.1% of conductance (bottom). $\overline{g_{Na}}$ = 600 pS µm^{-2} and 341 pS µm^{-2}, respectively. Note that the latency between the two voltage signals increases, as observed experimentally.
(**c**) Plot of reliability of AP propagation, shown as color coding of the surface of the reconstructed neuron for $\overline{g_{Na}}$ = 500 pS µm^{-2}. Color scale bar indicates the reliability of propagation in the axon (inset, top); dendrites are depicted in black to indicate lack of active AP propagation. Gray sphere represents the proximal region of the axon. Axonal recording pipette on an 8th order axon branch is illustrated schematically.
(**d**) Plot of latency against distance for $\overline{g_{Na}}$ = 500 pS µm^{-2}. Color scale bar indicates axon branch order (inset, top). Dashed lines indicate the results of linear regression for distances > 100 µm.
(**e**, **f**) Contour plots of reliability (**e**) and velocity (**f**) of AP propagation for the experimentally recorded cell. Note that the reliability of AP propagation is supported above a critical value of $\overline{g_{Na}}$ = 200 pS µm^{-2}, whereas the speed of propagation further increases at supercritical values of $\overline{g_{Na}}$ > 200 pS µm^{-2}. Gray scale bar indicates the value of the indicated parameter (right).

Supplementary Table 1 Density and functional properties of Na^+ channels in BC axons.

Parameter	Axon	Soma
$\overline{g_{Na}}$ [a]	310.7 ± 32.7 pS µm^{-2} (n = 37) 574.3 ± 120.8 pS µm^{-2} (n = 11)	31.9 ± 3.7 pS µm^{-2} (n = 24)
Single Na^+ channel conductance (0 mV) [b]	12.5 ± 1.0 pS (n = 5)	
Open probability Na^+ channels (0 mV) [b]	0.66 ± 0.05 (n = 5)	
Na^+ channel density [a]	25.0 channels µm^{-2} (n = 37) 46.1 channels µm^{-2} (n = 11)	2.6 channels µm^{-2} (n = 24)
Activation time constant (0 mV) [c, d]	64 ± 6 µs (n = 4)	122 ± 34 (n = 9)
Inactivation time constant (0 mV) [c]	303 ± 21 µs (n = 11)	728 ± 98 µs (n = 9)
Midpoint potential activation curve [e]	–42.0 ± 0.7 mV (n = 14)	–31.1 ± 1.3 mV (n = 11)
Slope factor activation curve [e]	7.3 ± 0.5 mV (n = 14)	9.8 ± 0.9 mV (n = 11)
Midpoint potential inactivation curve [e]	–76.6 ± 1.0 mV (n = 13)	–72.1 ± 1.5 mV (n = 6)
Slope factor inactivation curve [e]	8.4 ± 0.6 mV (n = 13)	9.3 ± 1.2 mV (n = 6)
Total surface area of BC axon [f]	40546 µm^2	
Total estimated number of Na^+ channels in BC axon [g]	~1.9 x 10^6	

a Boundary between proximal and distal compartment was set at a distance of 100 µm from axon origin.
b Values determined by nonstationary fluctuation analysis[26,44]; conductance value represents chord conductance.
c For activation and inactivation time constant analysis, only experiments with peak currents > 20 pA were included.
d For measuring activation time constant, only experiments sampled at 100 kHz were included.
e Error estimates were obtained by bootstrap analysis.
f Axonal surface area of BCs according to Nörenberg et al.[9]
g Based on Na^+ channel density in distal axon.